energies

MDPI

Article

Influence of Low-Temperature Charge on the Mechanical Integrity Behavior of 18650 Lithium-Ion Battery Cells Subject to Lateral Compression

Zhenhai Gao [1], Xiaoting Zhang [1], Yang Xiao [1,*], Hao Gao [1], Huiyuan Wang [2] and Changhao Piao [3]

[1] State Key Laboratory of Automobile Simulation and Control, Jilin University, Changchun 130025, China; gaozh@jlu.edu.cn (Z.G.); xiaotingzhang3@sina.com (X.Z.); gaohao2019@163.com (H.G.)
[2] School of Materials Science and Engineering, Jilin University, Changchun 130025, China; wanghuiyuan@jlu.edu.cn
[3] School of Automation, Chongqing University of Posts and Telecommunications, Chongqing 400000, China; piaoch@cqupt.edu.cn
* Correspondence: xiaoy2016@jlu.edu.cn; Tel.: +86-431-8509-4353

Received: 25 December 2018; Accepted: 22 February 2019; Published: 27 February 2019

Abstract: The study on the damage tolerance and failure mechanism of lithium-ion batteries (LIBs) subject to mechanical attack has attracted considerable attention. The electrochemical performance and thermal behavior of LIB were significantly affected by operation temperature and charging rate, but the dependence of these two factors on mechanical response remains unclear. Hence, we investigated how the environmental temperatures and rates in charging process affected the mechanical response characteristics of 18650 LIB cells. The onset of the short circuit in the cells which charged at temperatures above −25 °C occurred around their modulus peak under compression. At −25 °C, there was a strong possibility that a premature short circuit occurred locally in the cells during charging, thus they might show complex and variable mechanical response under compression. The failure moduli and crushing stresses of cells subject to compression tended to decrease as their ambient charging temperatures went down. Besides, 0.5 C-charged cells exhibited higher failure moduli and crushing stresses than the 1 C-charged cells above −20 °C. Morphology analyses of the cell electrode surfaces revealed that mossy lithium deposits became evident at temperatures below −10 °C. Furthermore, their distribution was uniform. Mechanical results also indicated that the short-term cycling at −20 °C and 0.5 C would soften the cell.

Keywords: lithium-ion battery; mechanical integrity behavior; low-temperature charge; charging rate

1. Introduction

With the steadily increasing energy density, power density and cycle life, as well as the sustained decline in cost, the applications of lithium-ion batteries (LIBs) have been expanded from consumer electronics to hybrid and fully electric vehicles (HEVs and EVs) [1,2]. Compared with conventional petrol vehicles, new energy vehicles will inevitably bring new security risks [3,4]. In recent years, there have been some reports that the batteries in electric vehicles, such as Chevy Volt and Tesla Model S, caught fire when subjected to collisions or foreign object intrusion. Along with the possession quantity and the rapid increase of electric vehicles, the likelihood of such accidents occurred during vehicle movement will continuously increase. Hence, it is essential to study the mechanical failure and thermal runaway of batteries subjected to mechanical load [5,6]. The study of the mechanical response of a battery cell at macroscale will provide information on the load capacity of its structure. Also, the study at microscale will contribute to a deeper understanding of the mechanical failure mechanism.

To maximize the life and security of LIBs, the methods of operation have to be optimized [7–9]. Choi et al. revealed that the cycle-life of LIBs was mainly influenced by their charge conditions, but was relatively insensitive to their discharge conditions [10]. Besides, charging conditions are less dependent on diversified demands than the discharge conditions [9]. Thus, the design of battery charging protocol should be investigated in detail. Xu et al. extensively studied the static and dynamic mechanical properties of cylindrical 18650 cells and their dependency on the state of charge (SOC) and the cycle-life [11–13]. Their test result indicated that the short circuit fault of the cells with higher SOC (lower than 80%) occurred at higher modulus and smaller strain. Research by Tsutsui et al. confirmed the conclusions of Xu et al. [14]. They believed that the SOC of 18650 cells affected their stiffness, but had little effect on their mechanical failure load. Recently, our group has investigated the influence of the charging cut-off voltage on the mechanical integrity behavior of 18650 lithium-ion cells [15]. The result showed that the cells with high charging voltage were prone to fail at small moduli and stresses, and the thermal runaway risk of a cell would be 100% when its voltage exceeded 4.4 V. For the pouch cells, the test results revealed that their SOC dependence could be negligible under indentation loads [16]. This suggested that the SOC dependence of the mechanical behavior of lithium-ion cells may be related to their shapes, structures and manufacturing processes. In fact, besides the SOC, there are many other variable conditions that should be studied to provide a reference for optimizing the charging protocol, such as charging temperature, humidity, rate and so on [17–19]. Many studies have reported the mechanical behavior of the battery components under these conditions [20–23]. Nevertheless, relevant reports of battery cells are few.

In terms of large-scale industrial applications, power batteries are required to operate at a wide range of temperatures. For example, many reports have pointed out that the batteries of plug-in HEVs and EVs should be able to charge at −30 °C and survive at −46 °C [24,25]. At low temperatures, the diffusion rate of Li^+ in the electrolyte and the solid-electrolyte-interphase (SEI) film during charging, the charge transfer rate of Li^+ at the interface of the anode/ SEI film, and the diffusion rate of Li^+ in the solid anode material are reduced, which will greatly increase the electrochemical polarization and concentration polarization of LIBs. The polarizations of LIBs will not only decrease their actual capacity, but also will cause that the potential at the interface of the anode/SEI film to be lower than the potential of the Li/Li^+ reaction, eventually leading to the deposition of lithium at the interface of the anode/SEI film [26,27]. The deposited lithium will react with the electrolyte and form the electrically insulating dead lithium during cycling, resulting in irreversible loss of active lithium and accelerating cell aging. Besides, the dendritic lithium on the anode surface is extremely easy to pierce the separator, which can cause a severe local short circuit. These factors must give new features to the mechanical response of the cells after low-temperature charging as compared to that of the cells after room-temperature charging. Therefore, it is very important to study the impact of low temperature charging on the mechanical response of the battery cell. Recently, Friesen et al. conducted nail penetration tests on the LIB cells with and without experiencing aging at low temperature [28]. Their test result showed that the cells after low-temperature cycles had a higher thermal runaway risk. However, the quantitative relationships between mechanical behaviors and their charging temperature, charging rate and cycle number at low temperatures were still lacking. The study of the influence of the temperature, charging rate and cycle number on cell mechanical behaviors contributes to further understanding of its crash safety and improve its model prediction. In this paper, we tested the mechanical behavior of 18650 battery cells charged at various temperatures (−25 °C, −20 °C, −15 °C, −10 °C and 25 °C) under lateral compression. The charging currents were specified to be 0.5 C and 1 C. Furthermore, the lateral compression of the cells experiencing cycling at −20 °C and 0.5 C were conducted to obtain the impact of the low-temperature cycle on their mechanical response. The voltage drop of the cell was monitored to speculate the occurrence of its internal electrical short circuit which was considered as its mechanical failure point.

2. Materials and Methods

2.1. Experimental Object

Ternary materials are the most promising cathode materials of the LIBs in electric vehicles owing to their high energy and power density. $LiCoO_2$ component in ternary cathode materials (a multi-component system $LiNiO_2-LiCoO_2-LiMnO_2$ or $LiNiO_2-LiCoO_2-LiAlO_2$) is essential because cobalt can enhance their electrochemical activity, electronic conductivity, and structural stability [29,30]. In this work, the most common commercial SONY 18650 LIB cells with a single chemical component $LiCoO_2$ were chosen to specialize and simplify the influences of electrode material on their mechanical response. The rated capacity and the maximum allowable charge current of these cells were 2.15 Ah and 2.15 A, respectively. Their lower and upper cut-off voltages were 2.5 and 4.2 V, respectively.

2.2. Electrochemical Measurements

The constant-current constant-voltage (CCCV) charge/discharge measurements were performed on the battery cell test system (BK-6808, Mingyu Equipment Co., Ltd., Shenzhen, China). First, two CCCV cycles of the cells at 0.2 C were conducted at normal temperature (25 °C) to obtain their state of health (SOH). Then, the cells were transferred to an environment chamber (FB-WGD4010, Hongyun Equipment Co., Ltd., Shanghai, China) to rest 10 h at a specified temperature. After that, the cells were charged at a specified rate to 4.2 V and maintained at 4.2 V until the charging current dropped below C/20. The surface temperatures of the cells during charging were measured by three DS18B20 digital temperature sensors (Sinachip Electronics Co., Ltd., Nanjing, China) and the three sensors were placed along the axial direction of a battery cell, as shown in Figure 1. For the cyclic aging, the test protocol was in accordance with that presented above. The aging was interrupted after every cycle for the SOH test at normal temperature (25 °C). After low-temperature charge, the cells were kept at room temperature for 24 h until their temperature restore to room temperature, then a digital voltmeter (34411A, Keysight Technologies, Santa Rosa, California, USA) was used to measure their ohmic resistance.

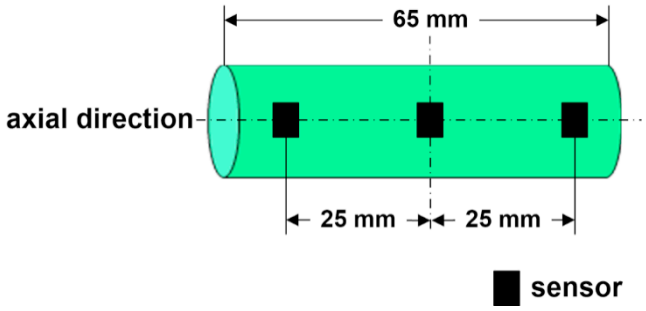

Figure 1. Positions of temperature sensor attachments.

2.3. Mechanical Testing

As shown in Figure 2a, the lateral compression of battery cell between two flat steel plates was carried out on a universal material testing machine (WAW-200, Fangrui Technology Co., Ltd., Changchun, China) at room temperature. The maximum load of this machine was 200 kN. The loading speed was set to 0.05 mm/s to create a quasi-static loading condition. The compression tests were terminated either until the cell resistance to load suddenly dropped or upon reaching the maximum load (200 kN). During the compression test, the cell voltage and its surface temperature were respectively recorded by a digital voltmeter and an infrared thermal camera (E95, FLIR, Portland, OR, USA). The test range of the camera was tuned to 0 °C–600 °C. Two or more repeated tests were conducted in each case to obtain sufficiently reliable results.

To obtain mechanical behavior of an 18650 LIB cell, the cylindrical cell body was considered as a whole frame (Figure 2b). A rather simple but useful method was used to convert the loading force–displacement curve obtained by compression into the nominal relationships between stress and strain, and between modulus and strain [11,12,15]. Nominal stress can be expressed as:

$$\sigma = \frac{F}{S}, \tag{1}$$

where F is the machine loading force, and S represents the contact area. S can be obtained as:

$$S = lb, \tag{2}$$

where l refers to the cylindrical axis length of the cell, and b indicates the contact width; b is estimated by using:

$$b = 2R\arccos\left(\frac{R - s/2}{R}\right), \tag{3}$$

where R denotes the radius of the cell, and s is the displacement of the indenter. Nominal strain can be expressed as:

$$\varepsilon = \frac{s}{2R}. \tag{4}$$

Accordingly, the compression modulus can be calculated by using:

$$E = \frac{d\sigma}{d\varepsilon}. \tag{5}$$

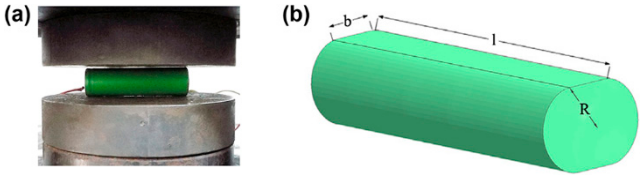

Figure 2. (**a**) Photograph of a pressure head of the universal testing machine and (**b**) schematic of a cylindrical cell during compressing.

2.4. Post-Mortem Analysis

An electrical circular saw was used to disassemble the battery cells treated at low temperatures. For safety consideration, all cells were disassembled after they were completely discharged (0% SOC) at room temperature. After that, the jellyroll inside the cell was carefully unwound and sampled. Samples of anode coating and separator were further characterized by the field emission scanning electron microscopy (FESEM, JSM-6700F, JEOL Ltd., Dongjing, Japan) to observe their surface morphology changes.

3. Results

3.1. Mechanical Characterization via Lateral Compression

Figure 3Aa,Ba, respectively, show nominal stress-time, nominal modulus-time, voltage-time and surface temperature-time curves of the 18650 LIB cells charged at −25 °C at 0.5 C and 1 C under compression. Figure 3Ab,Ac,Ad,Bb,Bc,Bd show the thermal images during compression, which respectively correspond to the letters marked in Figure 3Aa,Ba. The cells subject to compression could undergo a thermal runaway reaction. When thermal runaway of a cylindrical LIB cell occurred, the flame, smoke and debris were generally ejected from the safety valve of its positive end.

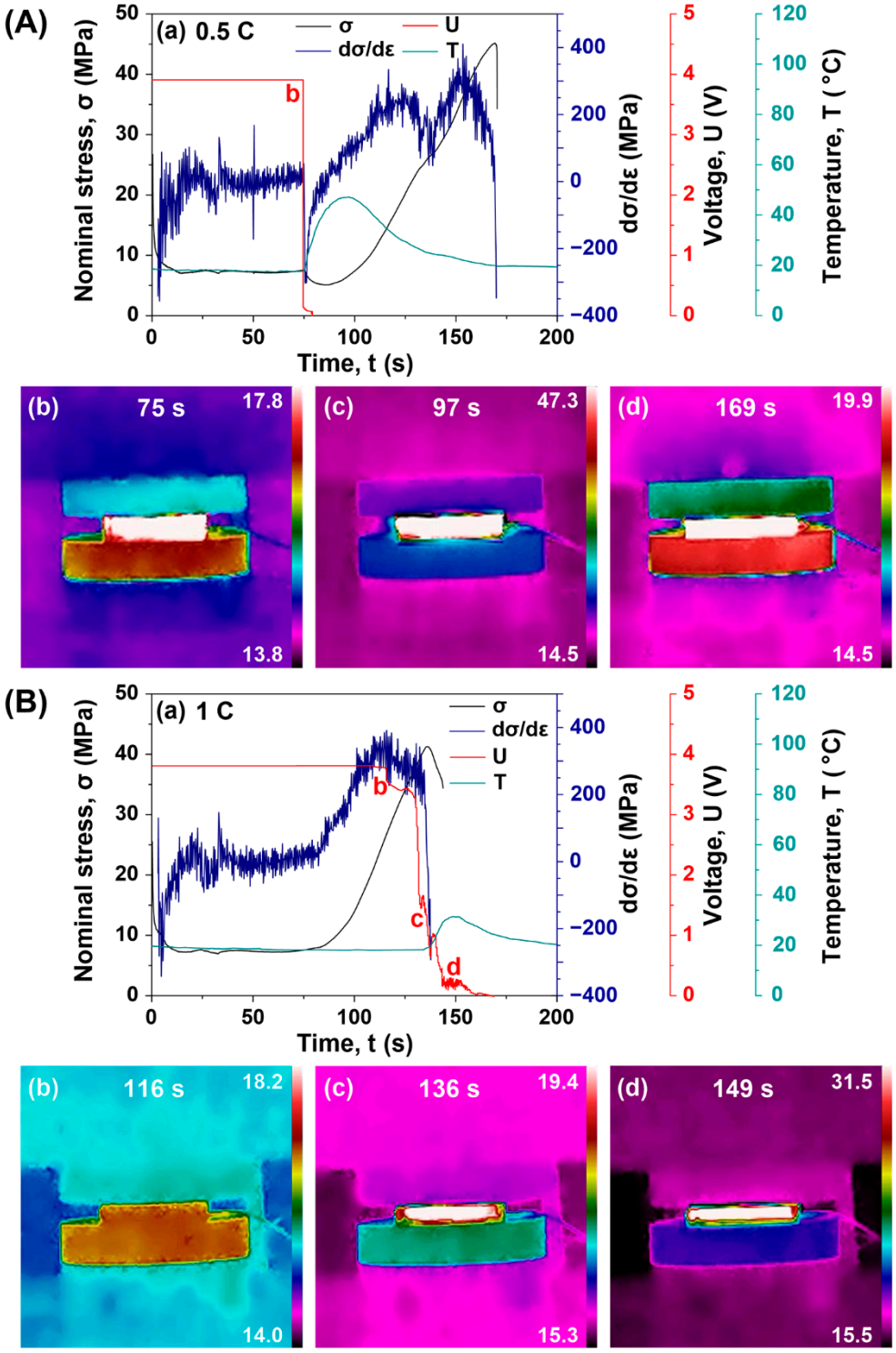

Figure 3. (**a**) The nominal stress-time, nominal modulus-time, voltage-time, and surface temperature-time curves in compression of the 18650 lithium-ion battery cells charged at −25 °C, and (**b**–**d**) their time-stamped thermal images: the cells (**A**) at 0.5 C and (**B**) at 1 C.

Hence, the temperature change of a small area between its center and its positive end was recorded to represent that of the entire cell in this study. In Figure 3Aa, the stress and the modulus of the cell remained basically unchanged after a short period of fluctuation at the initial stage of load, which was caused by the gap between casing and jellyroll, the gap between layers of the jellyroll, and the gap in the hollow center of winding steel needle [11]. After these gaps were eliminated, there were three

large fluctuations appearing in the modulus-time curve of the cell. At the first fluctuation, the load stress and the modulus of the cell suddenly decreased, and its voltage dropped to zero, suggesting that the cell was completely short circuited. Simultaneously, the outline of the cell body was clearly in its thermal image, and its surface temperature was 17.8 °C (Figure 3Ab). After that, its surface temperature slowly rose to 47.3 °C due to the large voltage drop (Figure 2Ac). During the temperature rising of the cell, its stress and modulus gradually increased. In the cooling process, its modulus decreased again, which was caused that the heat accumulated inside the cell was much enough to soften its structure. A period of time later, the modulus of the cell began to increase again until the cell reached its crushing phase. When the structure of the cell was completely crushed, its surface temperature was 19.9 °C (Figure 3Ad), and finally dropped to the room temperature. The cell was safe. For the cell charged at 1 C, its nominal stress-time, nominal modulus-time, voltage-time and surface temperature-time curves were presented in Figure 3Ba. After densification, the stress and modulus of the cell increased rapidly. When its modulus reached near the peak, the cell was completely compacted and then had a significant voltage drop, indicating that a partial internal short circuit had occurred [11,31]. At this moment, the surface temperature of the cell was maintained at around 17 °C (Figure 3Bb). After that, the temperature did not change along with the occurrence of the internal short circuit. It might be because this small voltage drop did not generate enough heat inside the cell to change its surface temperature. When the stress of the cell reached the peak, its modulus dropped sharply and its structure was crushed. Before that, the cell voltage showed a significant decrease, and gradually decreased to near zero. During this period, the outline of the cell body became clear in its thermal image (Figure 3Bc). This large voltage drop generated a large amount of heat inside the cell, and made its surface temperature rise rapidly to 31.5 °C (Figure 3Bd). After a few seconds, the surface temperature slowly decreased to room temperature. The cell was safe. A closer look at the changes of the cell voltage and modulus in the Figure 3Ba revealed that besides of the two significant voltage drops, the cell voltage also had some small drops owing to the fluctuations in its modulus. This indicated that multiple complex micro-shorts occurred inside the cell during compression, which might be related to the asymmetry of the cell caused by its cathode and anode tabs, the winding structure of the jellyroll, and the impurities introduced during the cell preparation process.

Both at 0.5 C and at 1 C, the cells charged at an environmental temperature above −25 °C exhibited a mechanical response similar to that of a cell charged at −25 °C at 1 C in our experiments. The nominal stress-time, nominal modulus-time, voltage-time, and surface temperature-time curves of these cells during compression were similar to those shown in Figure 3Ba. That was to say, the onsets of the internal short circuit of these cells were all near the peaks of their modulus. We considered the onset of the internal short circuit of a LIB cell as the critical point of its damage failure. Therefore, except for the cells charged at −25 °C at 0.5 C, the failure critical points of the other cells under compression were all near the peaks of their modulus. This conclusion was consistent with the test results of the cells charged to various states at ordinary temperature [11,15]. The cells charged at 0.5 C always exhibited more complex and variable mechanical response and their failure critical points were always at the first large fluctuating peaks of their moduli. Besides, the crushing stresses of the integral structure for all the test cells were at their stress peaks. In our experiments, we also found that the cells after low-temperature charge did not have a thermal runaway phenomenon under compression, and the probability of thermal runaway of the cells charged at 25 °C under compression was rather high. For the safety and unsafety cells after charged at 25 °C, their electrical, force and thermal changes during compression could be found in our previous study [15].

Figure 4 presents the nominal stress-strain and nominal modulus-strain curves of the cells charged at various environmental temperatures and rates. The nominal stress-strain curves of the cells charged at 0.5 C and 1 C were presented in Figure 4a,b, respectively. It could be seen from the two figures that at the same strain, the lower the charge environment temperature of the cell, the lower its load stress was.

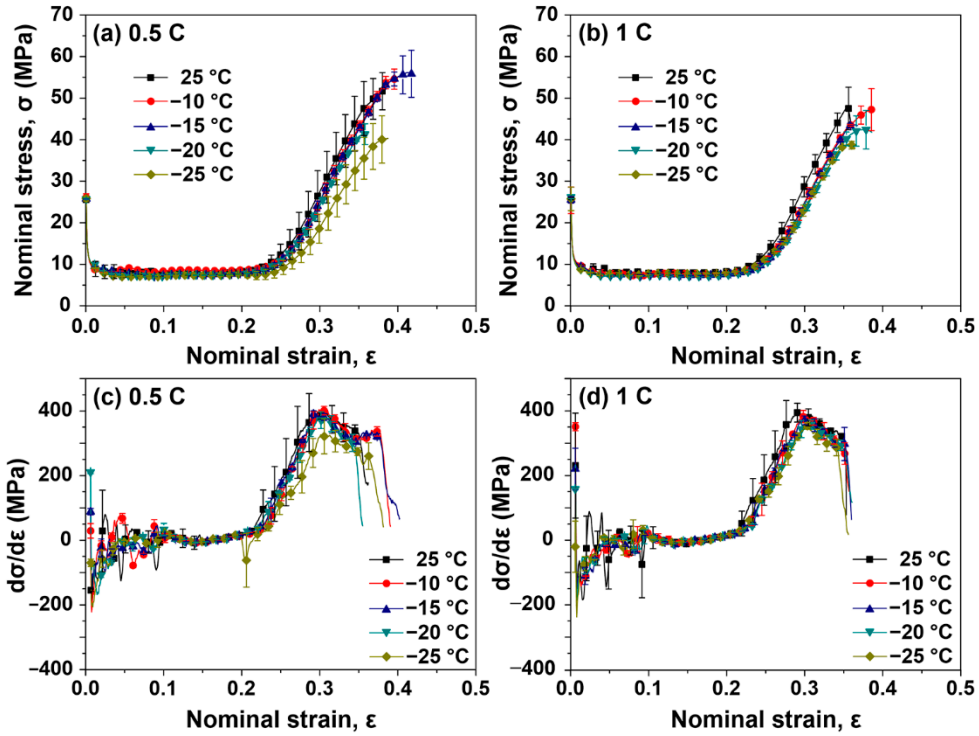

Figure 4. Nominal stress–strain and nominal modulus–strain curves of the 18650 lithium-ion battery cells charged at various environmental temperatures and rates.

Nominal modulus-strain curves of the cells were obtained by deriving their nominal stress-strain curves. The nominal modulus-strain curves of the cells charged at 0.5 C and 1 C were displayed in Figure 4c,d, respectively. From the two figures, we could find that at the same strain, the lower the charging environment temperature of the cell, the lower its modulus was. Both the load stress and modulus of the cell decreased with the charge environment. It indicated that the low-temperature charge softened the cell to various degrees, and softening degree increased with the charging environmental temperature. In order to more intuitively and clearly observe the impact of charging environment temperature and charging rate on their structural stiffness, the maximum modulus and the maximum load stress values of the cells charged at various environmental temperatures and rates were showed in the bar figures (Figure 5a,b). Observing the two figures, the maximum modulus and the maximum load stress values of the cells at the two rates tended to decrease with their charging environmental temperatures. The trend was more obvious when the charging rate was 1 C. This conclusion agreed with the observation from Figure 4. It demonstrated that a lower charging environmental temperature would soften the cell and made it can be crushed by a lower load. It also could be found from Figure 5a,b that the 0.5 C-charged cells exhibited higher maximum modulus and maximum stress values than the 1 C-charged cells at the low temperatures above −20 °C. Based on the analysis of Figure 3, we had known that for most of LIB cells, their failure critical moduli under compression were near their modulus peaks, and the crushing stresses of their integral structure were at their stress peaks. Specifically, the failure critical moduli of the cells charged at −25 °C and 0.5 C might be at the first large fluctuating peaks of their moduli, and their failure critical moduli were much smaller than their maximum moduli. Therefore, it could be concluded that the failure moduli and crushing stresses of the cells subject to compression tended to decrease with their charging environmental temperatures. In addition, the 0.5 C-charged cells exhibited higher failure moduli and crushing stresses than the 1 C-charged cells at the low temperatures above −20 °C.

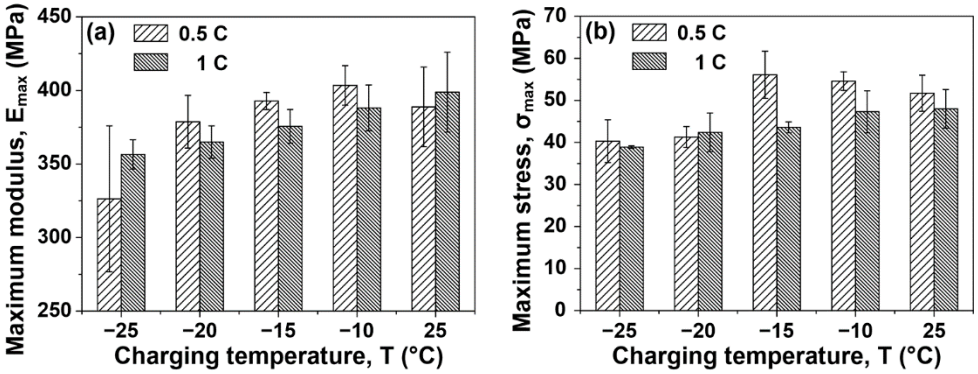

Figure 5. Relationships between the charging environmental temperatures and charging rates of 18650 LIB cells and their (**a**) maximum nominal moduli E_{max} and (**b**) maximum load stresses σ_{max}.

3.2. Electrochemical Characterization

Figure 6a–j, respectively, display voltage-time current-time and surface temperature-time curves of 18650 LIB cells during charging at 0.5 C and 1 C. At 0.5 C, comparing the voltage-time curves obtained at various environmental temperatures, we could find that the constant-current (CC) period at low temperatures became shorter than that at normal temperature. The lower the environmental temperature, the shorter the CC period was. It was because the severe electrochemical polarization and concentration polarization at low temperatures made the cells reach their charge cut-off voltage prematurely, and the lower the environmental temperature, the more severe the polarization was [26,27]. Specifically, the voltage curve of the cell at −15 °C showed a fluctuation in its initial stage of charging, which was caused by the generation and mitigation of cell polarization. This was also the cause of the appearance of a small fluctuation in the voltage curve of the cell at −20 °C. At −25 °C, the CC period disappeared in the voltage-curve of the cell, indicating that its polarization was intensified. It was worth noting that the current curve of the cell charged at −25 °C had two peaks, and at its second current peak the surface temperature rise of the cell was much higher than those of the other cells. Therefore, it could be concluded that the first current peak resulted from the mitigation and generation of the cell polarization, and the second current peak was caused by the generation and mitigation of the cell internal short circuit. For the cells charged at 1 C, their voltage curves almost had no CC period during low-temperature charging. It suggested that the polarization of the cells charged at 1 C was more serious than those charged at 0.5 C. Fluctuations in the current curves of these cells were also caused by the generation and mitigation of cell polarization. Observing the surface temperature and current curves of all the cells during charging, we found that the surface temperature of a cell always changed with its charging current.

When the environmental temperature was higher than −20 °C, the surface temperature of the cells increased with their charging rate. This was because the ohmic resistance of these cells was not dependent on their charging rate (Table 1). The higher the charging rate was, the more ohmic heat ($Q = I^2Rt$) of the cells produced. At −20 °C, the influence of the charging rate of the cells on their surface temperature was little, which was related to their small charging current and small ohmic resistance. In particular, the surface temperature of the cells during charging at −25 °C was mainly affected by the degree of their inner short circuit, which was dependent on the charging rate. In our tests, a lower charging rate always easily led to a more severe inner short circuit of the LIB cell, thus more heat accumulated in the cell, resulting in the higher rise of its surface temperature and structure softening.

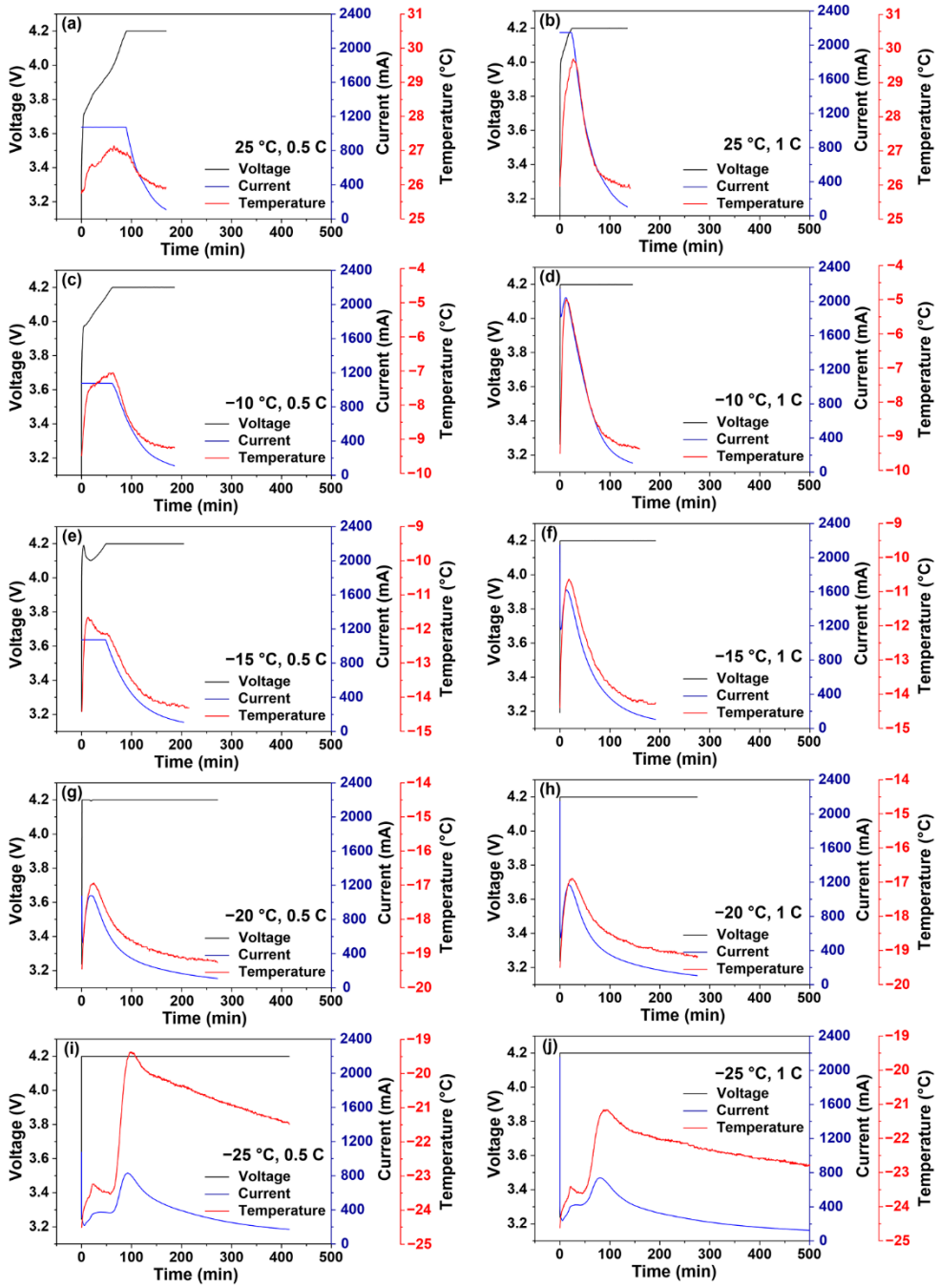

Figure 6. Voltage–time, current–time and surface temperature–time curves of the 18650 lithium-ion battery cells during charging at various environmental temperatures and rates.

Table 1. Average ohmic resistance of 18650 LIB cells after charging at various environmental temperatures and rates.

Charging Rate	Average Ohmic Resistance (mΩ)				
	25 °C	−10 °C	−15 °C	−20 °C	−25 °C
0.5 C	47.6	41.2	40.0	37.2	35.2
1 C	47.5	41.1	40.1	37.2	36.7

The voltage-capacity curves of the 18650 LIB cells during charging at various environmental temperatures and rates (0.5 C and 1 C) as well as the curves of discharging at normal temperature at 0.2 C were combined in Figure 7a,b. It could be found from the discharge curves of the test cells that their actual states of charge after charging decreased with the charging environmental temperatures both at 0.5 C and at 1 C. According to the study of Xu et al. [11], the modulus and load force of a cell decreased with its state of charge, which might be ascribed to the higher stiffness of the higher lithiation anode and the higher delithiation cathode [32–34]. This explained why the moduli and load stresses of the cells charged at both rates decreased with their charging environmental temperatures. The final display capacities of the cells charged at various environmental temperatures and their actual charge capacities were further presented by bar figures (Figure 7c,d). When the charge environment temperatures of the cells were higher than −25 °C, both their final charge display capacities and their actual charge capacities decreased with the charge environment temperatures. At −25 °C, the final charge display capacities of the cells were even higher than those of the cells charged at normal temperature and always reached the capacity warning value of 2580 mAh. It suggested that the cells after charging at −25 °C had been internally short circuited, resulting in that their actual voltages could not reach the preset value and then they were charged endlessly. This result was consistent with the analysis result of the current and surface temperature curves of the cells charged at −25 °C in Figure 6i,j. There was not much difference between the actual charge capacities of the cells after charging at 0.5 C and 1 C at the same environmental temperature. However, the temperature of the cells increased with their charging rate at the environmental temperatures higher than −20 °C. Hence, when the environmental temperature was higher than −20 °C, the failure moduli and crushing stresses of the cells charged at 0.5 C were visibly larger than those of the cells charged at 1 C. To quantify the irreversible capacity loss caused by side reactions and the formation of dead lithium during low-temperature charge, the states of health (SOH) of the cells before and after charging at 0.5 C and 1 C were respectively presented in Figure 7e,f. At both rates, the SOHs of the cells obviously were shortened when their charging environmental temperatures decreased. It indicated the irreversible lithium loss in the cells increased markedly with the decrease of their charging environmental temperatures, which was a reason why the actual charge capacity of the cells decreased with their environmental temperatures.

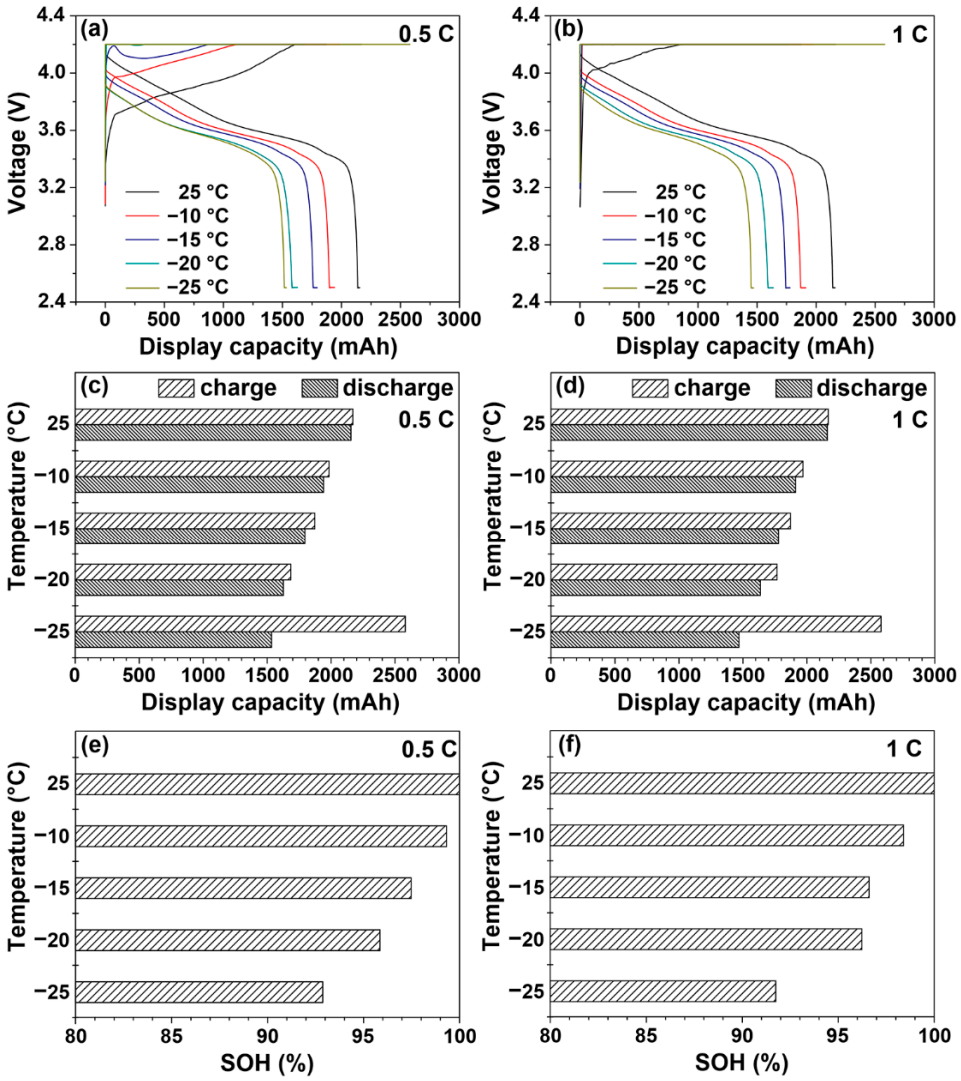

Figure 7. Charge curves at various environmental temperatures (**a**) at 0.5 C and (**b**) at 1 C, and discharge curves at 25 °C at 0.2 C of 18650 lithium-ion battery cells. Final charge and discharge display capacity of these cells: (**c**) at 0.5 C and (**d**) at 1 C. The state of health (SOH) for these cells after charging: (**e**) at 0.5 C and (**f**) at 1 C.

3.3. Morphology Characterization

The cells after charging at 1 C at various environmental temperatures were dismantled to understand the effect of low-temperature charge on their electrode surface status. There was no evident distinction between the electrode surface morphology of the cells after charging at 0.5 C and 1 C, and the key factor determining their electrode surface morphology was their charging environment temperatures. For the sake of brevity of presentation, only photographs and FESEM images of the cell electrodes after charging at 1 C were analyzed in detail in this paper.

Figure 8 showed the photographs of the anode and the separator (anode side) for the cells after charging at various environmental temperatures. At the environmental temperature below −10 °C, some yellow stains could be detected on the anode surfaces and the separator surfaces of the cells. The appearance of these yellow stains was caused by the lithiation of graphite and the plating/stripping of lithium metal [35–37]. For the cells after charging at −20 °C, the coverage of the yellow stains on its anode surface and separator surface became rather high. This phenomenon could be explained by the lithium ion diffusion rate in the cells at the temperature was very low, thus many lithium ions accumulated on their anode surface, resulting in increasing the degree of the lithiation of graphite

surface [36]. When the environmental temperature decreased to −25 °C, we found that the anode and the separator were tightly attached in the process of disassembling. After peeling off, the surface of the separator was still adhered with a very thin layer of anode coating (Figure 8j). There were a few yellow stains that can be clearly observed on the surfaces of the anode and the separator. This might be due to severe Li plating occurred the anode surface of the cells during charging at −25 °C, and the heat generated by the reaction of the deposited lithium metal and electrolyte made the anode and separator be bonded together. The supposition could be confirmed by the test results of their SOH. In order to further observe the effect of low-temperature charge on the micro-morphology of the cell electrode, FESEM images of the anode and separator surfaces of the cells after charging at 1 C at various environmental temperatures were presented in Figure 9. Figure 9a,b,e,f,i,j,m,n,q,r were the FESEM images of the anode surface of the cells after charging at 25 °C, −10 °C, −15 °C, −20°C and −25 °C, respectively. The FESEM images of the separator surface of the cells after charging at the five temperatures could refer to Figure 9c,d,g,h,k,l,o,p,s,t. Observing the FESEM images of the cell anode surfaces could know that the surface of the graphite particles became rough after low-temperature charging, and its roughness increased with the decrease of the charging environmental temperature. It might be related to the volume change of graphite particles caused by charging difficulties at low temperatures and the reaction between the deposited lithium and electrolyte. Especially at −20 °C and −25 °C, there were many small particles attached to the graphite particle surface. These small particles were either the reactants of the deposited lithium and electrolyte or the dead lithium formed during lithium plating and stripping [36]. From the FESEM images of the cell separator surfaces, we could find that when the charging environmental temperature was below −10 °C, some evident deposits appeared on the surface separator, which corresponded to the yellow stains on the separator surface in the photographs (Figure 8). At −25 °C, the separator surface was covered by a dense thin coating, which explained that the small particles attached on the anode surface of the cells after charging at −25 °C were less evident than those after charging at −20 °C. Through the observation of the macroscopic and microscopic morphology of the cell electrodes, it could be concluded that the lithium deposits formed during the low-temperature charging were uniformly distributed and their structure was mossy not dendritic, which was the reason why the test cells charged at low temperatures and normal temperature usually exhibited the similar mechanical response [38]. When the environmental temperature was as low as −25 °C, lithium deposits were adhered on the separator tightly, and it suggested that there was a strong possibility that a premature contact between the anode and the cathode occurred locally during charging. Thus, the cell was extremely prone to partial internal short circuit during charging, resulting in that the charging display capacity of the cell reached the warning value.

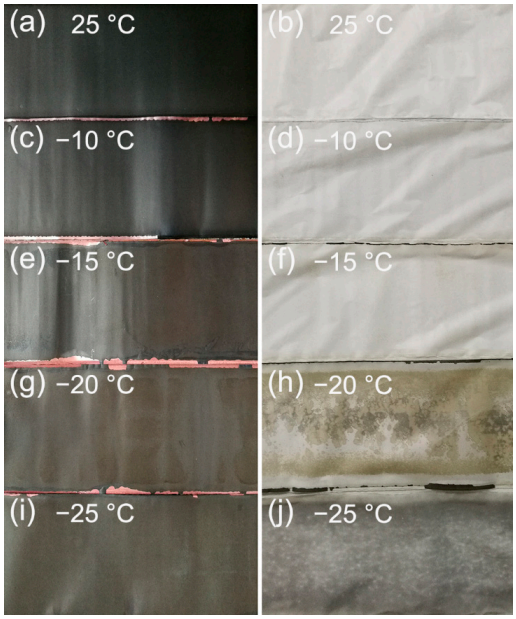

Figure 8. Photographs of the anode surfaces (left side) and separator surfaces (right side) dismantled from the 18650 lithium-ion battery cells after charging at 1 C, and the environmental temperatures were set to (**a**,**b**) 25 °C, (**c**,**d**) −10 °C, (**e**,**f**) −15 °C, (**g**,**h**) −20 °C and (**i**,**j**) −25 °C.

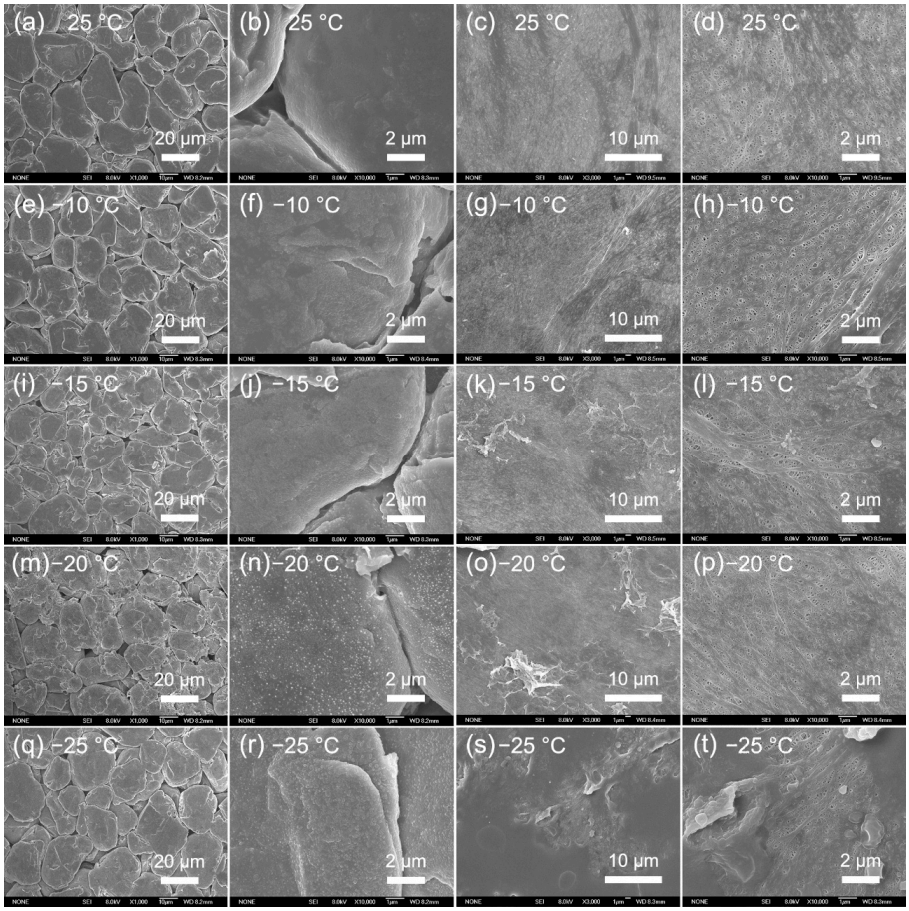

Figure 9. Field emission scanning electron microscopy (FESEM) images of the anode surfaces (left side) and separator surfaces (right side) dismantled from the 18650 lithium-ion battery cells after charging at 1 C, and the environmental temperatures were set to (**a**–**d**) 25 °C, (**e**–**h**) −10 °C, (**i**–**l**) −15 °C, (**m**–**p**) −20 °C and (**q**–**t**) −25 °C.

3.4. The Influence of Short-Term Cycle

We selected the LIB cells before and after short-term cycle at −20 °C and 0.5 C to investigate the influence of low-temperature aging on their mechanical behavior. For the cells before and after cycling, the changing curves of nominal stress, nominal modulus, voltage, as well as surface temperature with time during compression were similar.

The onset of short circuit in the cells after cycling was also near their modulus peaks. Figure 10a,c, respectively, show the nominal stress–strain curves and nominal modulus–strain curves of the charged cells in the first and 20th cycles under compression. Twenty low-temperature cycles made the cell achieve densification earlier, which might result from the increasing plating lithium on the anode surface of the cell during cycling. It was clear that the cells after cycling had lower maximum modulus and higher maximum load stress than those before cycling. It suggested that the low-temperature cycle softened the cells and increased the crushing difficulty of their structure. The voltage-time, current-time, and surface temperature-time curves of the cells in the first and 20th cycles were displayed in Figure 10b, and their actual capacity and average ohmic resistance were presented in Table 2. We found that the actual capacity, charging current and ohmic resistance of the cell decreased significantly after cycling, but the surface temperature rise of the cell in the 20th cycle was higher than that of the cell in the first cycle. This demonstrated that the exothermic side reactions in the cell after cycling increased greatly. Observing the relationship between the SOH value of the cells and their cycling number (Figure 10d), it could be found that the test cells had reached the end of their life in the 20 cycles, indicating that the exothermic side reactions of the plating lithium and electrolyte and the formation of dead lithium were sever during cycling.

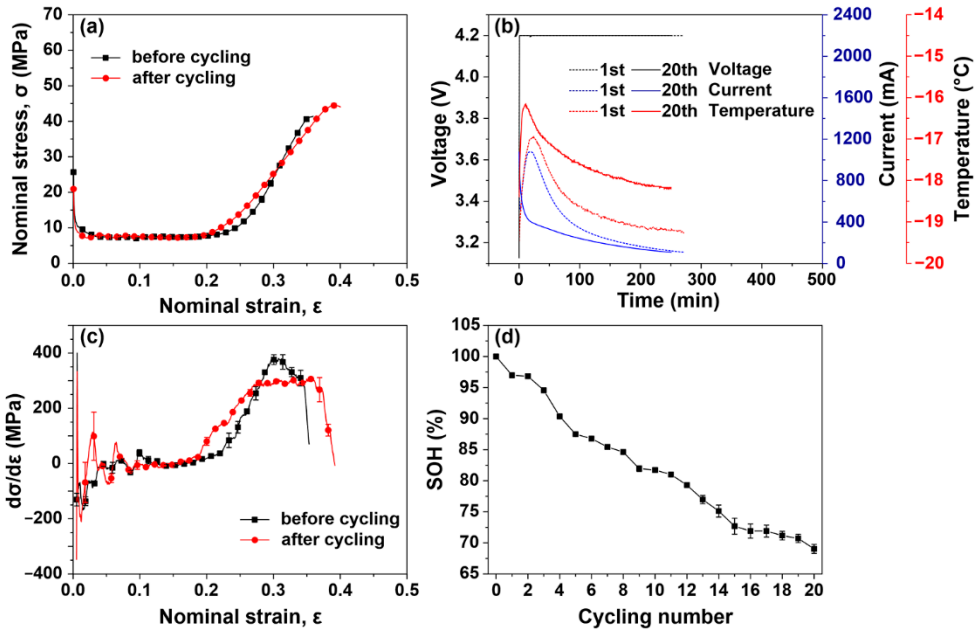

Figure 10. (**a**) Nominal stress–strain curves, (**b**) voltage–time, current–time and surface temperature–time curves, and (**c**) nominal modulus–strain curves of the 18650 lithium-ion battery cells before and after cycling at −20 °C and 0.5 C. (**d**) The SOH of the cells during the cycling.

Table 2. Actual charge capacity and average ohmic resistance of charged 18650 LIB cells in the first and 20th cycles.

Cycling Number	Actual Charge Capacity (mAh)	Average Ohmic Resistance (mΩ)
1	1626.3	37.2
20	1078.0	25.1

The decreased actual charge capacity and the increased exothermic side reactions were both the reasons why the short-term cycle at −20 °C and 0.5 C made the cell become soft. Moreover, the effect of the cycle on the morphology of cell electrode was little.

4. Discussion

In summary, we investigated the mechanical response characteristics of 18650 LIB cells after charging at 0.5 C and 1 C at various environmental temperatures. The temperatures used in this study were 25 °C, −10 °C, −15 °C, −20 °C and −25 °C, and then − 20 °C was selected to further study the influence of low-temperature cycle on the mechanical response of cells.

Mechanical compression results demonstrated that the onset of a short circuit in the cells, which were charged at environmental temperatures above −25 °C, occurred around their modulus peaks. When the environmental temperature decreased to −25 °C, the LIB cells suffered severe deterioration of the cell-to-cell uniformity, and there was a strong possibility that a premature short circuit occurred locally during charging, resulting in that their charge display capacity reached the warning value. At −25 °C, the mechanical response of the cells during charging was mainly affected by the degree of their inner short circuit. According to our test result, a lower charging rate always easily led to a more severe inner short circuit of the cell, thus more heat accumulated in the cell, resulting in the higher rise of its surface temperature and structure softening. The cells charged at −25 °C at 1 C always had similar mechanical behavior with the cells charged at environmental temperatures above −25 °C. However, the cells charged at −25 °C at 0.5 C always exhibited more complex and variable mechanical response and their failure critical points were always at the first large fluctuating peaks of their moduli.

The onset of the internal short circuit of a LIB cell could be considered as the critical point of its damage failure. The failure critical modulus of the cell under compression was near its modulus peak, and the crushing stress of its integral structure was at its stress peak. Mechanical test results also showed that the failure moduli and crushing stresses of the cells subject to compression tended to decrease with their charging environmental temperatures. This was mainly because the actual states of charge for the cells after charging decreased with their charging environmental temperatures due to the increase of polarization and irreversible lithium loss at lower temperatures. Besides, at the low temperatures above −20 °C, the 0.5 C-charged cells exhibited higher failure modulus and crushing stress values than the 1 C-charged cells, because the higher charging rate could increase ohmic heat.

Macroscopic and microscopic morphology analysis of the cell anode and separator surfaces revealed that lithium deposits became evident when the environmental temperature was below −10 °C. The distribution of the lithium deposits on the anode and separator surfaces was uniform and their structure was mossy not dendritic, which was the reason why the test cells after charging at low temperatures usually exhibited the similar mechanical response with the cells after charging at normal temperature. It was noteworthy that the thermal runaway risk of the cells after charging at low temperatures under compression was low owing to its low actual charge capacity and uniformity of lithium deposition.

Furthermore, the onset of short circuit of the cells after a short-term cycle at −20 °C and 0.5 C also occurred near their modulus peaks. The decreased actual charge capacity and the increased exothermic side reactions for the cells after low-temperature cycle led to their integral structure softening.

This study may provide some valuable insights for understanding the relationship between electrochemical behavior at low temperatures of LIBs and their mechanical response, and build a foundation for the research about LIB crash-safety. Due to the limitations of our experimental condition, this study only investigated the mechanical characterization at room temperature. In our future work, the mechanical tests of the cells at various environmental temperatures should be carried out to simulate the actual working condition.

Author Contributions: Conceptualization, Z.G.; Data curation, H.G.; Resources, H.W.; Supervision, C.P.; Writing–original draft, X.Z.; Writing–review & editing, Y.X.

Funding: This work was supported by the State Key Laboratory of Automotive Simulation and Control Open Foundation (20180102), the National Science Foundation of China (No. 51705190), and the National Key Research and Development Program of China (No. 2017YFB0102600).

Conflicts of Interest: The authors declare no conflict of interest.

References

1. Zhao, R.H.; Guo, S. Comprehensive Performance Assessment on Various Battery Energy Storage Systems. *Energies* **2018**, *11*, 2841. [CrossRef]
2. Andwari, A.M.; Pesiridis, A.; Rajoo, S.; Martinez-Botas, R.; Esfahanian, V. A Review of Battery Electric Vehicle Technology and Readiness Levels. *Renew. Sustain. Energy Rev.* **2017**, *78*, 414–430. [CrossRef]
3. Zhu, J.; Wierzbicki, T.; Li, W. A Review of Safety-Focused Mechanical Modeling of Commercial Lithium-Ion Batteries. *J. Power Sources* **2018**, *378*, 153–168. [CrossRef]
4. Kong, L.; Li, C.; Jiang, J.; Pecht, M.G. Li-Ion Battery Fire Hazards and Safety Strategies. *Energies* **2018**, *11*, 2191. [CrossRef]
5. Hooper, J.; Marco, J.; Chouchelamane, G.; Lyness, C.; Taylor, J. Vibration Durability Testing of Nickel Cobalt Aluminum Oxide (Nca) Lithium-Ion 18650 Battery Cells. *Energies* **2016**, *9*, 281. [CrossRef]
6. Hooper, J.; Marco, J.; Chouchelamane, G.; Lyness, C. Vibration Durability Testing of Nickel Manganese Cobalt Oxide (Nmc) Lithium-Ion 18,650 Battery Cells. *Energies* **2016**, *9*, 52. [CrossRef]
7. Amanor-Boadu, J.M.; Guiseppi-Elie, A.; Sanchez-Sinencio, E. The Impact of Pulse Charging Parameters on the Life Cycle of Lithium-Ion Polymer Batteries. *Energies* **2018**, *11*, 2162. [CrossRef]
8. Monem, M.A.; Trad, K.; Omar, N.; Hegazy, O.; Mantels, B.; Mulder, G.; Van den Bossche, P.; Van Mierlo, J. Lithium-Ion Batteries: Evaluation Study of Different Charging Methodologies Based on Aging Process. *Appl. Energy* **2015**, *152*, 143–155. [CrossRef]
9. Keil, P.; Jossen, A. Charging Protocols for Lithium-Ion Batteries and Their Impact on Cycle Life-an Experimental Study with Different 18650 High-Power Cells. *J. Energy Storage* **2016**, *6*, 125–141. [CrossRef]
10. Choi, S.S.; Lim, H.S. Factors That Affect Cycle-Life and Possible Degradation Mechanisms of a Li-Ion Cell Based on Licoo2. *J. Power Sources* **2002**, *111*, 130–136. [CrossRef]
11. Xu, J.; Liu, B.; Hu, D. State of Charge Dependent Mechanical Integrity Behavior of 18650 Lithium-Ion Batteries. *Sci. Rep.* **2016**, *6*, 21829. [CrossRef] [PubMed]
12. Xu, J.; Liu, B.; Wang, X.; Hu, D. Computational Model of 18650 Lithium-Ion Battery with Coupled Strain Rate and Soc Dependencies. *Appl. Energy* **2016**, *172*, 180–189. [CrossRef]
13. Xu, J.; Jia, Y.; Liu, B.; Zhao, H.; Yu, H.; Li, J.; Yin, S. Coupling Effect of State-of-Health and State-of-Charge on the Mechanical Integrity of Lithium-Ion Batteries. *Exp. Mech.* **2018**, *58*, 633–643. [CrossRef]
14. Tsutsui, W.; Siegmund, T.; Parab, N.D.; Liao, H.; Nguyen, T.N.; Chen, W. State-of-Charge and Deformation-Rate Dependent Mechanical Behavior of Electrochemical Cells. *Exp. Mech.* **2018**, *58*, 627–632. [CrossRef]
15. Gao, Z.; Zhang, X.; Xiao, Y.; Wang, H.; Li, N. Influence of Coupling of Overcharge State and Short-Term Cycle on the Mechanical Integrity Behavior of 18650 Li-Ion Batteries Subject to Lateral Compression. *Int. J. Hydrog. Energy* **2018**, *43*, 5261–5271. [CrossRef]
16. Luo, H.; Xia, Y.; Zhou, Q. Mechanical Damage in a Lithium-Ion Pouch Cell under Indentation Loads. *J. Power Sources* **2017**, *357*, 61–70. [CrossRef]
17. Kumar, A.S.; Satyavani, T.; Senthilkumar, M. Effect of Temperature and Charge Stand on Performance of Lithium-Ion Polymer Pouch Cell. *J. Energy Storage* **2016**, *6*, 239–247. [CrossRef]
18. Zhang, L.; Mu, Z.; Gao, X. Coupling Analysis and Performance Study of Commercial 18650 Lithium-Ion Batteries under Conditions of Temperature and Vibration. *Energies* **2018**, *11*, 2856. [CrossRef]
19. Rahimian, S.K.; Rayman, S.; White, R.E. Optimal Charge Rates for a Lithium Ion Cell. *J. Power Sources* **2011**, *196*, 10297–10304. [CrossRef]
20. Xu, J.; Wang, L.; Guan, J.; Yin, S. Coupled Effect of Strain Rate and Solvent on Dynamic Mechanical Behaviors of Separators in Lithium Ion Batteries. *Mater. Des.* **2016**, *95*, 319–328. [CrossRef]
21. Xu, C.; Ahmad, Z.; Aryanfar, A.; Viswanathan, V.; Greer, J.R. Enhanced Strength and Temperature Dependence of Mechanical Properties of Li at Small Scales and Its Implications for Li Metal Anodes. *Proc. Natl. Acad. Sci. USA* **2017**, *114*, 57–61. [CrossRef] [PubMed]

22. Haselrieder, W.; Westphal, B.; Bockholt, H.; Diener, A.; Höft, S.; Kwade, A. Measuring the Coating Adhesion Strength of Electrodes for Lithium-Ion Batteries. *Int. J. Adhes. Adhes.* **2015**, *60*, 1–8. [CrossRef]
23. Lin, Y.C.; Chen, X.-M. A Critical Review of Experimental Results and Constitutive Descriptions for Metals and Alloys in Hot Working. *Mater. Des.* **2011**, *32*, 1733–1759. [CrossRef]
24. Ji, Y.; Zhang, Y.; Wang, C.-Y. Li-Ion Cell Operation at Low Temperatures. *J. Electrochem. Soc.* **2013**, *160*, A636–A649. [CrossRef]
25. Zhang, J.; Jun, H.; Lufan, C.; Zhe, L. Lithium-Ion Battery Discharge Behaviors at Low Temperatures and Cell-to-Cell Uniformity. *J. Automot. Saf. Energy* **2014**, *5*, 391–400.
26. Li, Z.; Huang, J.; Liaw, B.Y.; Metzler, V.; Zhang, J. A Review of Lithium Deposition in Lithium-Ion and Lithium Metal Secondary Batteries. *J. Power Sources* **2014**, *254*, 168–182. [CrossRef]
27. Zhu, J.; Feng, J.; Guo, Z. In Situ Observation of Lithium Dendrite on the Electrode in a Lithium-Ion Battery. *Energy Storage Sci. Technol.* **2015**, *4*, 66–71.
28. Friesen, A.; Horsthemke, F.; Monnighoff, X.; Brunklaus, G.; Krafft, R.; Borner, M.; Risthaus, T.; Winter, M.; Schappacher, F.M. Impact of Cycling at Low Temperatures on the Safety Behavior of 18650-Type Lithium Ion Cells: Combined Study of Mechanical and Thermal Abuse Testing Accompanied by Post-Mortem Analysis. *J. Power Sources* **2016**, *334*, 1–11. [CrossRef]
29. Liu, Y.; Liu, M. Reproduction of Li Battery Linixmnyco1−X−Yo2 Positive Electrode Material from the Recycling of Waste Battery. *Int. J. Hydrog. Energy* **2017**, *42*, 18189–18195. [CrossRef]
30. Pişkin, B.; Aydinol, M.K. Development and Characterization of Layered Li(Nixmnyco1−X−Y)O2 Cathode Materials for Lithium Ion Batteries. *Int. J. Hydrog. Energy* **2016**, *41*, 9852–9859. [CrossRef]
31. Kisters, T.; Sahraei, E.; Wierzbicki, T. Dynamic Impact Tests on Lithium-Ion Cells. *Int. J. Impact Eng.* **2017**, *108*, 205–216. [CrossRef]
32. Sethuraman, V.A.; Chon, M.J.; Shimshak, M.; van Winkle, N.; Guduru, P.R. In Situ Measurement of Biaxial Modulus of Si Anode for Li-Ion Batteries. *Electrochem. Commun.* **2010**, *12*, 1614–1617. [CrossRef]
33. Qi, Y.; Guo, H.; Hector, L.G.; Timmons, A. Threefold Increase in the Young's Modulus of Graphite Negative Electrode During Lithium Intercalation. *J. Electrochem. Soc.* **2010**, *157*, A558. [CrossRef]
34. Amanieu, H.-Y.; Aramfard, M.; Rosato, D.; Batista, L.; Rabe, U.; Lupascu, D.C. Mechanical Properties of Commercial Lixmn2o4 Cathode under Different States of Charge. *Acta Mater.* **2015**, *89*, 153–162. [CrossRef]
35. Yuan, Q.F.; Zhao, F.; Wang, W.; Zhao, Y.; Liang, Z.; Yan, D. Overcharge Failure Investigation of Lithium-Ion Batteries. *Electrochim. Acta* **2015**, *178*, 682–688. [CrossRef]
36. Uhlmann, C.; Illig, J.; Ender, M.; Schuster, R.; Ivers-Tiffée, E. In Situ Detection of Lithium Metal Plating on Graphite in Experimental Cells. *J. Power Sources* **2015**, *279*, 428–438. [CrossRef]
37. Burns, J.C.; Stevens, D.A.; Dahn, J.R. In-Situ Detection of Lithium Plating Using High Precision Coulometry. *J. Electrochem. Soc.* **2015**, *162*, A959–A964. [CrossRef]
38. Petzl, M.; Danzer, M.A. Nondestructive Detection, Characterization, and Quantification of Lithium Plating in Commercial Lithium-Ion Batteries. *J. Power Sources* **2014**, *254*, 80–87. [CrossRef]